Chapter 3

SIDIS with CLAS12

Chapter 1 introduced polarized Semi-Inclusive Deep Inelastic Scattering (SIDIS) as a powerful tool for investigating the nucleon's internal structure, allowing access to the Transverse-Momentum-Dependent distributions (TMDs). This Chapter aims to outline a preliminary analysis of the Beam-Spin Asymmetry (BSA) associated with the structure-function $F_{LU}^{\sin\phi}$. It is treated as a case study ~~of~~ a possible measurement of non-perturbative QCD phenomena with flavor sensitivity, made possible by having an efficient PID apparatus. The analysis is performed on data acquired by the CLAS12 experiment at JLab, using the first module of the RICH installed in 2018; the second module was not available till the start of experiments with polarized targets in June 2022. It is based on the efficiency study reported in Chapter 2, which guarantees minimal pion contamination in the eK^+X sample. The study aims to show that it is possible to extract relevant observables with kaons, like the Beam-Spin Asymmetry, despite the reduction ~~of the~~ statistics ~~caused by the relatively smaller phase space covered by the RICH compared to the full CLAS12 spectrometer.~~ The SIDIS data selection criteria, the analysis method, and the results are included in this Chapter.

3.1 Data

The analyzed data belong to CLAS12 Run Group B (RG-B) and were acquired in the spring of 2019. The target was unpolarized liquid deuterium, and the longitudinally polarized electron beam was run at 10.6 GeV and 10.2 GeV with a current of 50 nA. The average beam polarization was $(84.8 \pm 1.5)\%$; it was monitored during the data-taking period by frequent measurements performed with the Moller polarimeter placed upstream CLAS12. The beam helicity was swapped with a frequency of 30 Hz to wash out detector effects and minimize the systematic effects. The torus magnet was full-field *inbending*, pushing positive particles forward outward.

The analysis is performed on positive kaons: the final state ~~is~~ eK^+X.

The standard CLAS12 reconstruction provides the electron identification and the kinematic of the particles, while it is expressly required that the RICH identify the kaon. These conditions reduce the available statistic because, at the time of data collection, only one of the six CLAS12 sectors was equipped with a RICH module. The analyzed data sample constitutes approximately one-third of the available statistics of electroproduction on deuterium and one-tenth of that on hydrogen and deuterium.

3.1.1 The CLAS12 SIDIS cuts

Electron related cuts

The final states, which include one electron and one positive kaon, are considered in this analysis. For the electron selection, the standard CLAS12 conditions for SIDIS were applied [36]:

- It has to be in the Forward Detector, i.e. the polar angle is between 5° and 40°.

- It has to be a trigger particle for the experiment.

- The number of photoelectrons in the HTCC has to be greater than 2.

- The energy in the PCAL has to be greater than $0.07\,\text{GeV}$.

- The DC fiducial cut developed for Run Group A was applied (running conditions were quite similar, except for the target that was hydrogen instead of deuterium).

- The z coordinate of track vertex was selected to be between $-8\,\text{mm}$ and $3\,\text{mm}$.

- The so-called "diagonal cut" is applied for the electron with momentum larger than $4.5\,\text{GeV}$. In this momentum range, the HTCC showed some inefficiency in distinguishing electron and pion, which can be cured using this cut based on the ratio of the energy deposed in the pre-shower and inner calorimeter.

- The ECAL fiducial cut, which allows to decrease the contamination of negative pion into the electron sample.

Hadron and RICH related cuts

Aiming to study the performance of the RICH, the following conditions were applied to the hadron:

- It has to be passed through sector 4 and identified by the RICH;

- Aiming to ~~show~~ the role of the RICH, the momentum is selected to be included in the detector working range $(3 \div 8\,\text{GeV})$;

- The number of photoelectrons in the RICH has to be greater than 2, to well-define the ring.

- The DC fiducial cut developed for Run Group A ~~was~~ applied (running conditions were quite similar, except for the target).

- The z coordinate of track vertex ~~was~~ selected to be between $-10\,\text{mm}$ and $2.5\,\text{mm}$.

- Having the particle trajectory a key role in the ring reconstruction, which is based on a ray-tracing algorithm, the fitted DC track has to have a reduced $\chi^2_{track} < 8$.

Kinematic cuts

After the selection of the electron and kaon, the following cuts based on the kinematic were applied:

- $y < 0.75$;

- $Q^2 > 1\,\text{GeV}^2$;

- $z > 0.2$;

- $x_F > 0.0$;

- $W > 2$;

- $MM > 1.6\,\text{GeV}$;

Remembering notation defined for SIDIS in Section 1.3,

$$\ell(l) + N(P) \rightarrow \ell(l') + H(p_H) + X \tag{3.1}$$

where the quantities in parentheses represent the four-momenta, the quantities on which the cuts are applied can be defined:

- Q is the transferred momentum;

$$Q = \sqrt{(l' - l)^2} = \sqrt{-q^2} \tag{3.2}$$

- y is the fraction of electron energy transferred to the target;

$$y = \frac{P \cdot q}{P \cdot l} \tag{3.3}$$

- z is the fraction of electron energy acquired by the kaon;

$$z = \frac{P \cdot p_H}{P \cdot q} \qquad (3.4)$$

- x_F is the so-called Feymann x, the fraction of the nucleon momentum carried by the parton struck by the electron;

$$x_F = \frac{2p_H \cdot q}{Q^2} \qquad (3.5)$$

- W is the center of mass energy

$$W = m_N^2 + 2m_N\nu - Q^2 \qquad (3.6)$$

where ν is the energy carried by the virtual photon;

- MM is the missing mass of the reaction.

$$MM = \sqrt{(E_{in} - E_{out})^2 - (\mathbf{p}_{in} - \mathbf{p}_{out})^2} \qquad (3.7)$$

Cuts effect

The effect of cuts is evaluated on the sample of events which include a $3 \div 8$ GeV K^+ identified by the RICH. This means that a strong reduction of the available CLAS12 statistics was already made because the RICH covers[1] one-sixth of the spectrometer.

The reduction of the statistics produced by each cut was evaluated by applying them separately to the full sample and checking the size of the final sub-sample. There are four main cuts, each saving approximately 50% of the events. Combining these four cuts, the subsample obtained consists of the 7.3% of the events. The other selection criteria, separately suppress $\sim 15\%$ of the original sample. Combining all cuts, the final subsample is made by 4.0% of the original sample. After applying these cuts, the final sample is composed of a few less than 2×10^5 events.

The most effective cuts are one related to the DC, two to the RICH data and reconstruction, and one to the kinematic. They respectively are:

- The DC fiducial cut for the hadron;

- the request of having at least three photons in the RICH. This can be affected by the unfinished alignment in the reconstruction software, missing part of the spherical mirrors, and consequently causing some photons to be lost;

- the cut on the track reduced χ_{track};

---

[1]At the time of data taking only one CLAS12 sector was equipped with the RICH
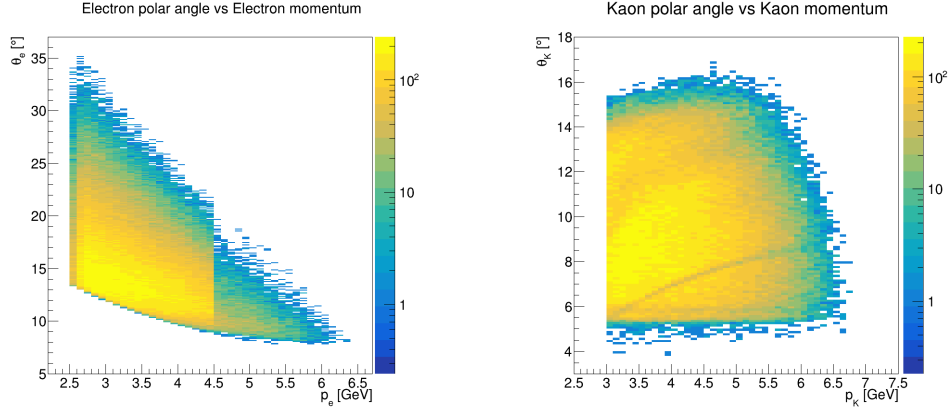
(a) Distribution of the polar angle and momentum of the selected electrons. The separation line visible at $4.5\,\text{GeV}$ is due to the "diagonal cut".

(b) Distribution of the polar angle and momentum of the selected kaons. The slightly darker line depends on the small separation between the two regions covered by the aerogel.

Figure 3.1: Phase space covered by the selected events.

- the cut on y.

The phase space covered by the particles surviving the selection is shown in Figure 3.1, while the distributions as a function of Q^2, x_B, z, p_T are represented in Figure 3.2.

3.2 Analysis

Since the available statistic is limited, the Unbinned Maximum Likelihood (UML) method was selected to obtain the measurement. With respect to the binned method, UML requires more computational resources but provides more reliable results in case of low statistics because it computes the asymmetry term event-by-event instead of using a cumulative histogram. The analysis software was developed by the author using `C++` and Clas12root, a framework derived from ROOT CERN that includes methods to read the CLAS12 data files, that are coded in binary HIghly Performance Output (HIPO) format.

3.2.1 The Unbinned Maximum Likelihood fit

The UML Fit method is based on the assumption that the Probability Density Function (PDF) associated with the i event has the same functional form of the cross-section

$$PDF(x_i, \alpha) = \frac{\sigma_{UU}(1 + A_i(\alpha))}{\mathcal{N}\left(\int d\sigma_{UU}\right)} \tag{3.8}$$
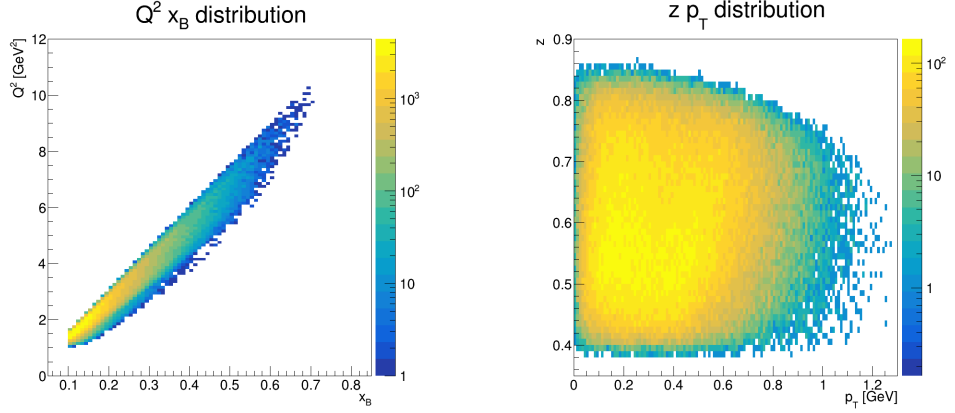
(a) Distribution of events as a function of the Q^2 and x_B variables.

(b) Distribution of events as a function of the z and p_T variables.

Figure 3.2: Distribution of events in the four-dimension of interest.

where x_i is the set of variables associated with the event, α is a set of parameters, $\mathcal{N}$ is a term depending on $\int d\sigma_{UU}$ to normalize the PDF to 1, σ_{UU} is the unpolarized cross-section, A_i is a term taking into account the wanted asymmetry, . If the unpolarized cross-section does not depend on the parameters of the fit, as it happens in this case, the PDF became

$$PDF(x_i, \alpha) = 1 + A_i(\alpha) \tag{3.9}$$

The likelihood function for a set of N events can be obtained as

$$\mathcal{L} = \prod_{i=1}^{N} PDF(x_i, \alpha) \tag{3.10}$$

Applying the logarithm to the $\mathcal{L}$ permits the transformation of the product into a sum, making easier the computation:

$$\log \mathcal{L} = \sum_{i}^{N} \log \left[PDF^{norm}(x_i, \alpha) \right] \tag{3.11}$$

Under the hypothesis of a large sample of independent measurements, the logarithm of the likelihood behaves like a chi^2.

$$\chi^2 = -2 \log \mathcal{L} \tag{3.12}$$

so it is possible to extract the most probable value of the asymmetry by minimizing the χ^2.

To extract the $A_{LU}^{\sin\phi}$ asymmetry, the PDF is

$$PDF_{\pm}(x_i, A_{LU}^{\sin\phi}) = 1 \pm P_b(A_{LU}^{\sin\phi} \sin\phi_i) \tag{3.13}$$

48

where the sign changes following the helicity of the beam, and P_b is the beam mean polarization. This PDF is automatically normalized, so it can be used directly in the definition of the likelihood

$$\log \mathcal{L} = \sum_{i}^{N^+ + N^-} \log \left[1 \pm P_b \left(A_{LU}^{\sin \phi} \sin \phi_i \right) \right] \tag{3.14}$$

The $F_{LU}^{\sin \phi}$ term is related to the BSA $A_{LU}^{\sin \phi}$ by equation

$$A_{LU}^{\sin \phi} = \frac{\sqrt{2\varepsilon(1-\varepsilon)}F_{LU}^{\sin \phi}}{F_{UU}} \tag{3.15}$$

where ε is a kinematic factor defined in Equation 1.12. Then, the likelihood is

$$\log \mathcal{L} = \sum_{i}^{N^+ + N^-} \log \left[1 \pm P_b \left(\frac{\sqrt{2\varepsilon(1-\varepsilon)}F_{LU}^{\sin \phi}}{F_{UU}} \sin \phi_i \right) \right] \tag{3.16}$$

and it is sufficient to minimize $-2\mathcal{L}$ to find the value of the structure-function ratio.

This method has the advantage of being independent of the binning in ϕ and provides results also if applied to relatively small samples. ~~Against~~ the UML method, ~~it~~ requires large computation resources to perform the minimization over thousands of events, and it is not always easy to define the PDF and its normalization. In the case of the extraction of $F_{LU}^{\sin \phi}$ for kaon, the ~~pros~~ appeared more relevant than the ~~cons~~, so the UML was selected.

3.2.2 UML fit validation

The UML fit was implemented using the ROOT::Math::Minimizer class, which allows the minimization of a function depending on one or more parameters. The software was validated on $e\pi^+ X$ data acquired ~~by the~~ Run Group A (RG-A), ~~which acquired data in similar conditions with respect to~~ RG-B but using hydrogen instead of deuterium as a target. To validate the analysis, the structure-function ratio $\frac{F_{LU}^{\sin \phi}}{F_{UU}}$ is extracted as a one-dimensional function of x_B, z, and p_T and compared with the published result. The validation process was performed using the CLAS12 reconstruction software, excluding the RICH, to have the same phase space ~~as~~ the original analysis. The comparison of the results is shown in Figures 3.3a, 3.3b, and 3.3c. Despite the plots ~~showing~~ a non-uniform systematic difference between the UML and published results, the trend of the functions ~~was~~ the same. ~~Probably this~~ discrepancy ~~was~~ due to ~~some~~ differences in the event selection of the two samples of pions. ~~This idea was confirmed by applying a~~ binned fit to the sample selected by the author, obtaining ~~more~~ similar results ~~with respect to the UML.~~ One example of the comparison is shown in Figures 3.4.
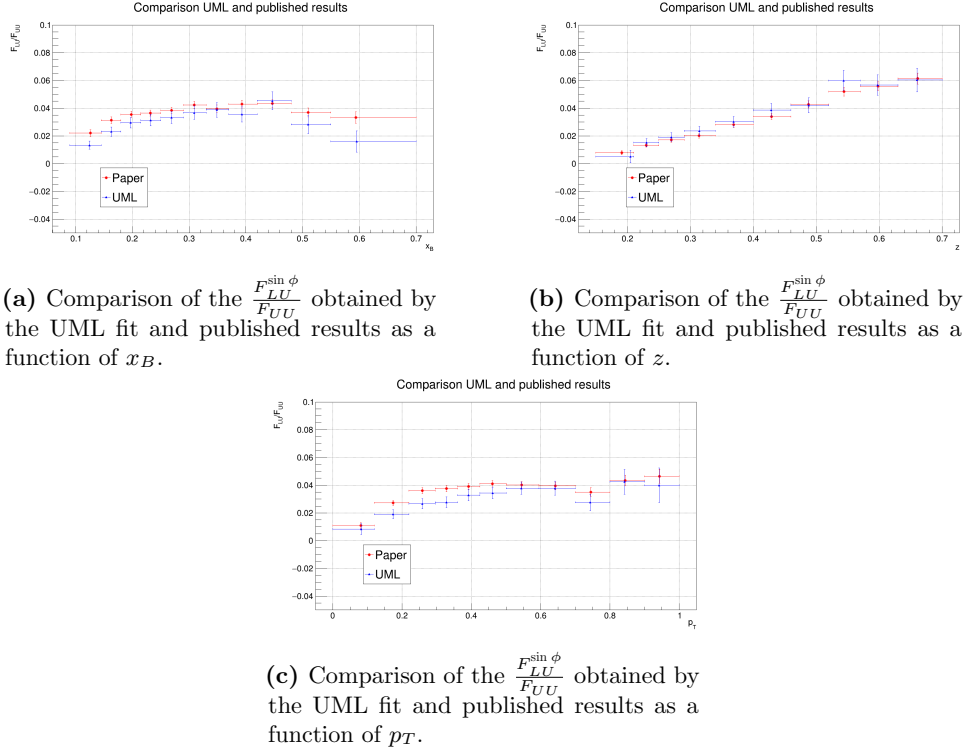
(a) Comparison of the $\frac{F_{LU}^{\sin\phi}}{F_{UU}}$ obtained by the UML fit and published results as a function of x_B.

(b) Comparison of the $\frac{F_{LU}^{\sin\phi}}{F_{UU}}$ obtained by the UML fit and published results as a function of z.

(c) Comparison of the $\frac{F_{LU}^{\sin\phi}}{F_{UU}}$ obtained by the UML fit and published results as a function of p_T.

Figure 3.3: One-dimensional comparisons of the $\frac{F_{LU}^{\sin\phi}}{F_{UU}}$ obtained by the UML fit and published results. The plots show a systematic difference between the two analyses. The one-dimensional plot as a function of Q^2 was not shown because it was not inserted in the Reference [39].

However, a small systematic difference was visible between the two methods. Theoretically, the UML fit should be better, because it does not suffer the binning effects. In any case, a systematic related to the extraction method was evaluated and described in the following. The implementation of the UML method is then working as expected and considered validated, and it was used to obtain any other results shown.

3.3 Systematic errors

The discussion of the systematic errors is still partially incomplete because the analysis started a few months before writing this document. It happened because the new version of the CLAS12 reconstruction software, the so-called Pass2, became available only after Summer 2023. Moreover, the CLAS12 simulation still does not include the RICH detector, making the estimation of the systematic more complex. For this reason, parts of the systematic reported in the following were taken from internal documents of the collaboration
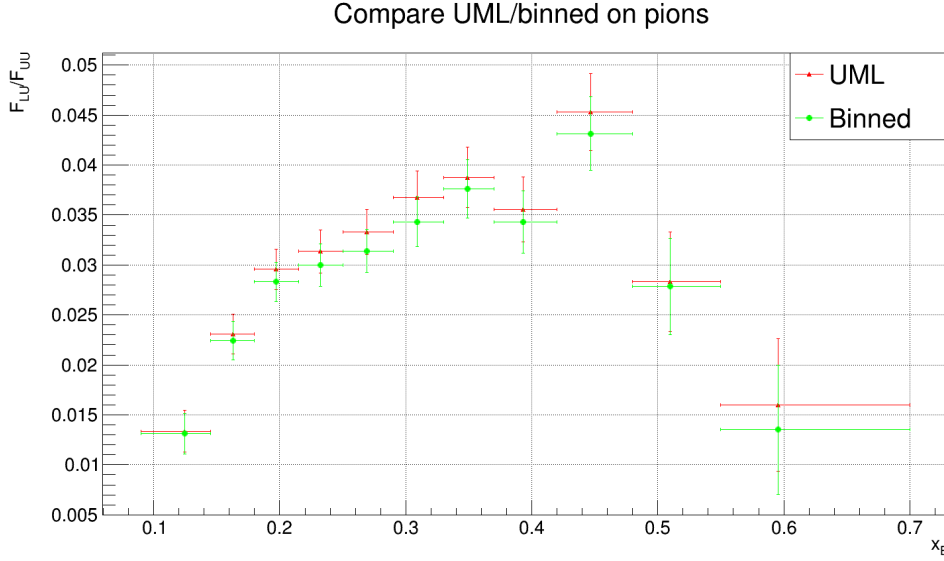
Figure 3.4: Example of the comparison between the $\frac{F_{LU}^{\sin\phi}}{F_{UU}}$ obtained by the UML fit and the binned fit applied to the same events, as a function of x_B. ~~However,~~ a small systematic difference is observed.

[49] and from the Reference reporting the CLAS12 results of pion BSA [39], having evaluated their values as reasonable. The systematic related to the identification of the kaon, which is related to the main subject of this thesis, was evaluated by exploiting the results of the efficiency study described in Section 2.4.

3.3.1 Main systematic uncertainties ~~imported from CLAS12~~

~~Uncertainty of the beam polarizaiton~~

The beam polarization was approximately weekly measured during the CLAS12 data taking. The measurements were performed using a Moller polarimeter, ~~which can be associated with~~ a systematic error of ~~the~~ 2%. This value has to be added in quadrature to the statistical error computed for the data sample considered. The statistical uncertainty associated with the RG-B data was 1.5%. The total uncertainty on the beam polarization is:

$$p_b = (84.8 \pm (stat)1.5 \pm (sys)2.0)\% = (84.8 \pm 2.5)\% \qquad (3.17)$$

The relative uncertainty on the beam polarization is used to define the correspondent systematic uncertainty on the structure-functions ratio:

$$\frac{\delta \frac{F_{LU}}{F_{UU}}}{\frac{F_{LU}}{F_{UU}}} = \frac{\delta A_{LU}^{\sin\phi}}{A_{LU}^{\sin\phi}} = \frac{\delta BSA}{BSA} = \frac{\delta p_b}{p_b} = 2.9\% \qquad (3.18)$$

51
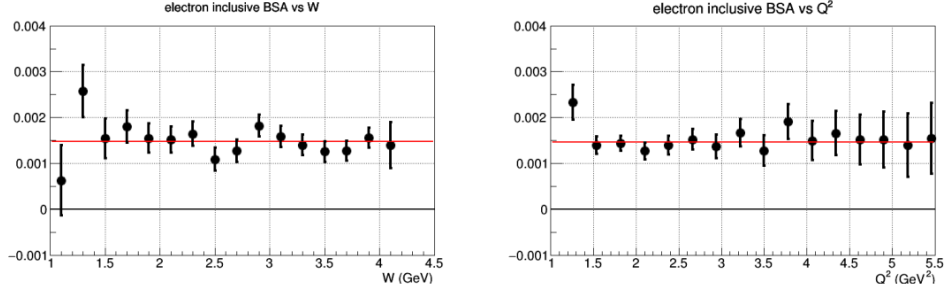
Figure 3.5: Systematic uncertainty associated with the charge beam helicity asymmetry. The plots are taken from the CLAS12 RG-A common analysis note [49].

Charge beam helicity asymmetry

The beam charge helicity correlated asymmetry was expected in CLAS12 to be at the level of 10^{-3}. It was estimated in the RG-A common analysis note [49] by checking the inclusive electron BSA. For the data acquired with ~~torus~~ configuration ~~inbending~~, this systematic is described by an additive term to the asymmetry ~~worth~~ +0.0015. Figure 3.5 contains the plots of this systematic error as a function of W and Q^2. To obtain the systematic uncertainty associated with the structure-function for each bin, this value was divided for the kinematic factor $\sqrt{\varepsilon(1-\varepsilon)}$, which relates $A_{LU}^{\sin\phi}$ and $\frac{F_{LU}^{\sin\phi}}{F_{UU}}$, computed using the mean value of ε. This systematic was compensated by applying an offset to the obtained value of the structure-function ratio. The offset value was ~ -0.003 for each bin. This systematic ~~error~~ was cured by adding the offset, and then it was excluded from the calculation of the global systematic uncertainty.

Acceptance and bin migration effects

The acceptance effects should be studied using the Monte Carlo (MC) by introducing a controlled asymmetry and comparing the structure-function ratio obtained using the generated and reconstructed particle by the simulation. This study could not be carried out because the RICH volume is not yet available in the CLAS12 MC. It is assumed that the estimation made for the pion cases can be a reasonable value, that can be used for this preliminary analysis. The relative uncertainty is set to 2.7%.

Radiative effects

The emission of a radiative photon in the scattering process introduces a mismatch between the virtual photon energy and the reconstructed value, this causes a bias on the SIDIS kinematic. Currently, there are no tools
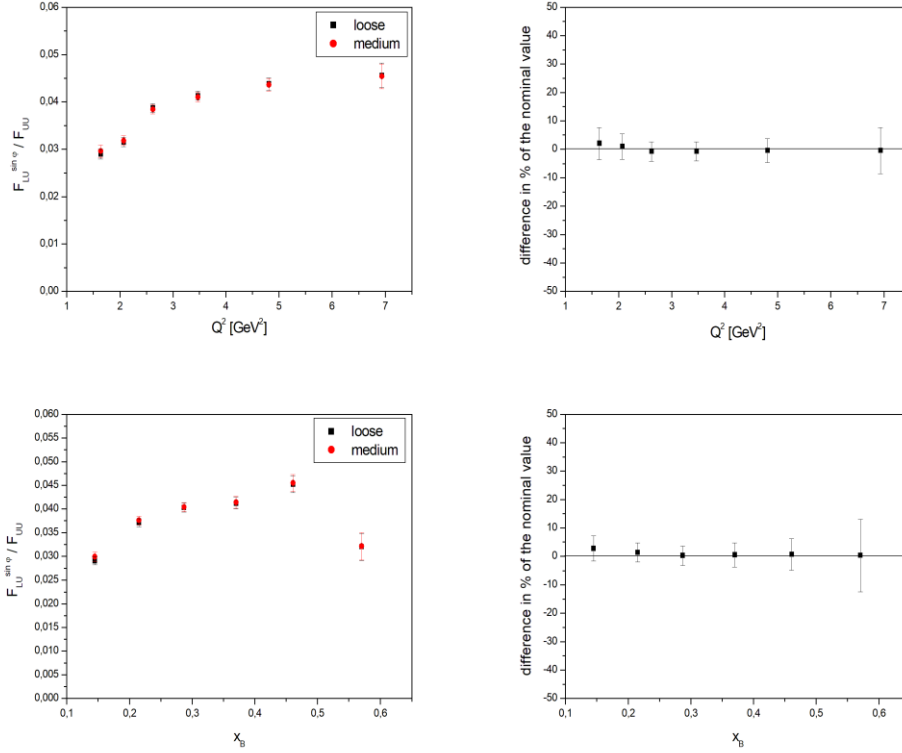
Figure 3.6: Plots describing the study on the effect the PCAL fiducial cut, taken from the CLAS12 RG-A common analysis note [49].

available to accurately estimate radiative effects for SIDIS BSA. The cuts on y and on MM, combined with the accessible values of z and p_T, minimize the contaminations from ~~exclusive radiative tail events~~. Moreover, the radiative effects are expected to be small in SIDIS processes ~~because of~~ the requirement of at least one hadron in the final state. For the case of pion, an estimation of the upper limit of the effect was performed using the dedicated software, setting this value at 3%. The analogous study for kaon is ~~still~~ missing, so for this preliminary study, the value estimated for pion was used.

Effects of fiducial cuts

The same fiducial cuts were applied to both the helicity states, and this effect was expected to be small. The main effect is related to the fiducial cut applied to the PCAL. By comparing the structure-function ratio for $e\pi^+X$ obtained by applying the loose and the medium cuts, as shown in Figure 3.6, the difference was found to be always less than the 5% and compatible with 0. ~~Then~~ this effect is neglected.

53
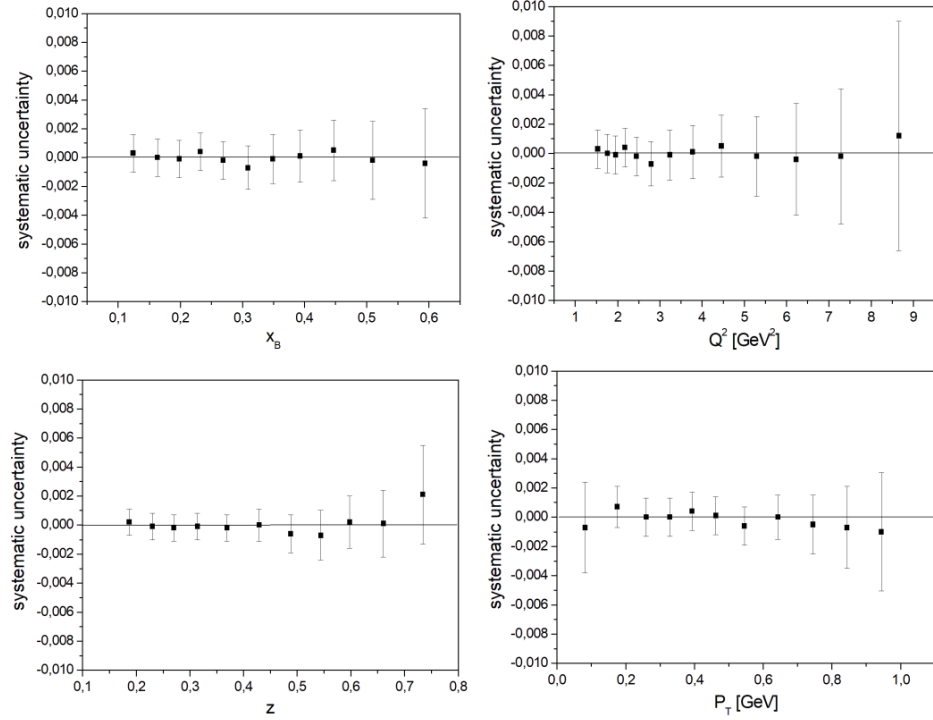
Figure 3.7: Systematic uncertainty associated with the π^- contamination into the e^- sample, taken from the CLAS12 RG-A common analysis note [49].

PID electron systematic effect

A possible source of systematic is the misidentification of negative pions as electrons. The diagonal and the ECAL fiducial cut reduce contamination by up to 2%. The systematic uncertainty associated with the pion contamination into the electron sample can be estimated only with the MC. It is assumed that the estimations made for the pion cases can be reasonable values, that can be used for this preliminary analysis. The relative uncertainty, as a function of x_B, Q^2, z, and p_T is shown in Figure 3.7. The effect is always comparable with zero, then it is neglected.

Extraction method systematic effect

Despite the previous consideration of expecting the UML fit theoretically better than the binned fit, it was decided to evaluate a systematic uncertainty depending on the extraction method, in case something in the implementation was not working as expected. For this reason, the systematic uncertainty was evaluated using the pion sample, which has larger statistics, to minimize the bins' effect on the binned method. The uncertainties were estimated from the plots like the one shown in Figure 3.4. The plots of the difference between
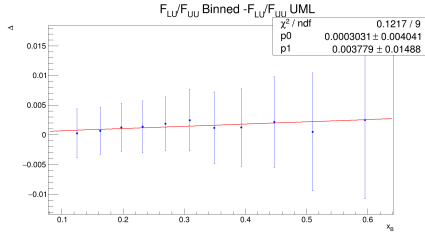
(a) Difference between UML and binned extraction results as a function of x_B.
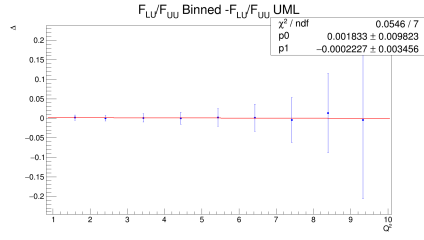
(b) Difference between UML and binned extraction results as a function of Q^2.
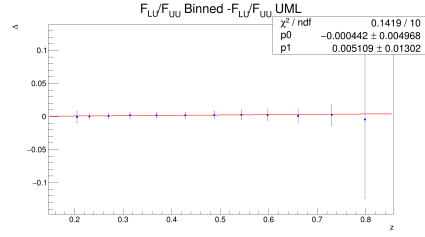
(c) Difference between UML and binned extraction results as a function of z.
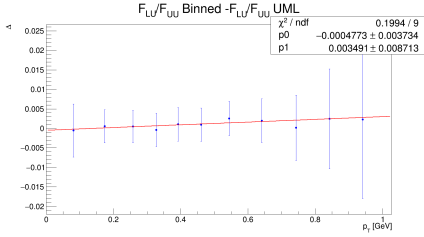
(d) Difference between UML and binned extraction results as a function of p_T.

Figure 3.8: Estimation of the systematic uncertainties related to the results extraction method.

~~the two methods results~~ were fitted using a linear function. This allows the estimation of a constant term and possibly dependence on the variables. The linear function describing the systematic uncertainty are shown in Figure 3.8. The ~~found~~ values of the parameters p_0 and p_1 ~~allow us to~~ neglect this source of systematic uncertainty.

3.3.2 Systematic uncertainty ~~caused by the kaon sample contamination~~

An upper limit of the systematic uncertainty on the structure-function ratio caused by the π^+ contaminating the K^+ sample was evaluated by exploiting the results of the efficiency study described in Section 2.4. To estimate the percentage of pions in the kaon sample, the RICH misidentification of pions $\eta_{\pi \to K}$ was used. This quantity depends on the hadron momentum, ~~and then~~ the hadron momentum distribution was used to weigh the different contributions:

$$r_\pi = \frac{\sum_i \eta_i n_{H,i}}{n_H} \tag{3.19}$$

The systematic uncertainty upper limit was evaluated using the $\frac{F_{LU}}{F_{UU}}$ values obtained for pions in the corresponding bin multiplied by the percentage of

pions:

$$\frac{\left(\delta\frac{F_{LU}}{F_{UU}}\right)_K}{\left(\frac{F_{LU}}{F_{UU}}\right)_K} = r_\pi \left(\frac{F_{LU}}{F_{UU}}\right)_\pi \tag{3.20}$$

where the pion structure-function ratio was obtained from the $e\pi^+X$ events satisfying the same selection criteria applied to the kaon sample; in particular, the pion was recognized by the RICH. These selection criteria were determined to select a comparable phase space. The plots showing the systematic uncertainty as a one-dimensional function were fitted with a first-order polynomial to highlight trends. The linear function, to which a cutoff at the 1% of relative error was added, was used to estimate punctually the systematic uncertainty. The systematic as a one-dimensional function of the electron and hadron variables are reported in Figures 3.9a, 3.9b, 3.9c, and 3.9d. For the four-dimensional analysis, the uncertainty derived from PID was estimated by evaluating it using the one-dimensional functions and the mean value of the corresponding variable computed for the bin and averaging over the four dimensions. The upper limit on the systematic uncertainty associated with contamination of kaons from pion is included in the range between the cutoff 1.0% and 2.6%. A more precise estimation could be done by assigning to the pion contamination a weight based on the difference between the measured structure-function ratio for kaon and pion rather than the entire value. The upper limit was considered enough because this is not the main source of systematic uncertainty, and the statistical error is more relevant in the case studied.

3.3.3   Global systematic uncertainty

Global systematic uncertainty is computed by adding all the sources of systematic uncertainty in quadrature. Table 3.1 recaps the results described previously. The relative systematic uncertainty is evaluated to be 5.3%. The upper limit of the systematic effect introduced by the contamination of pions in the kaon sample was evaluated to be, on average, the 2.0%, making it less relevant with respect to other sources of systematic uncertainties, which were estimated ~ 3% each. The systematic uncertainties are usually smaller rather than the statistical error, which is the dominating component of the measurement uncertainties. For this reason, a correction of the systematics effect was not developed, but they were simply added in quadrature to the statistical component.
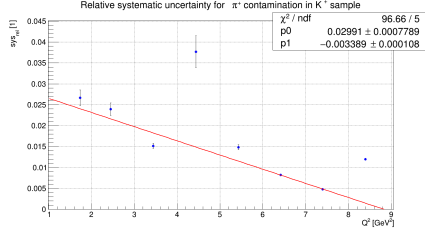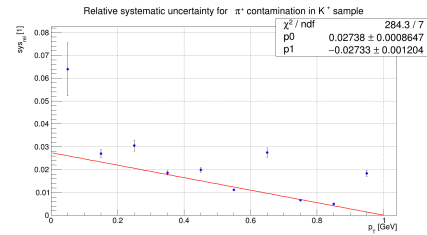
(a) Relative uncertainty associated with pion contamination into kaon sample.
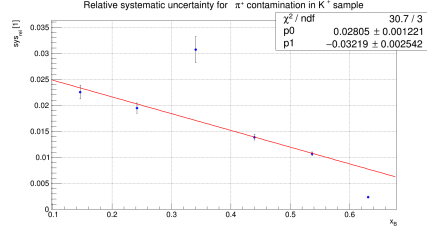
(b) Relative uncertainty associated with pion contamination into kaon sample.
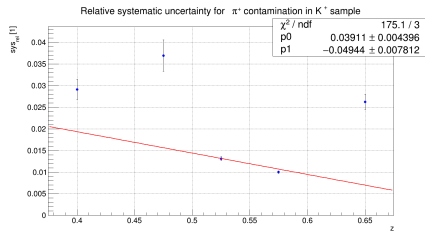
(c) Relative uncertainty associated with pion contamination into kaon sample.

(d) Relative uncertainty associated with pion contamination into kaon sample.

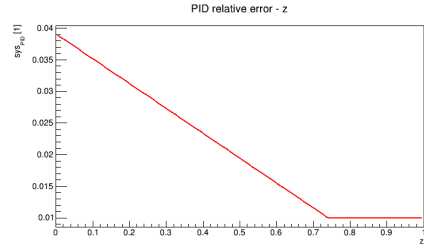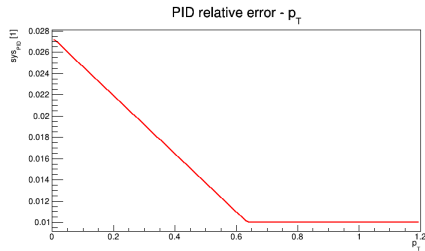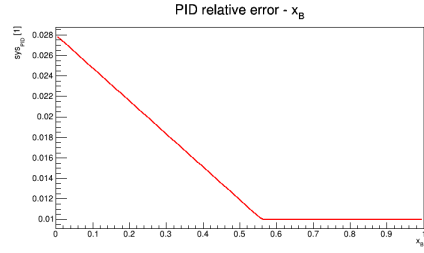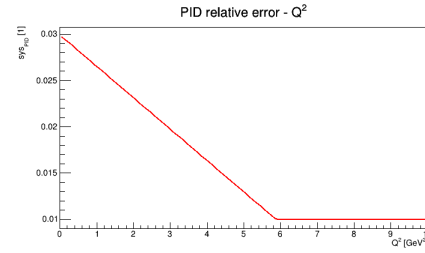**Figure 3.9:** Estimation of the PID systematic uncertainties related to the pion contamination into the kaon sample.

Figure 3.10: One-dimensional function found to evaluate the punctual systematic uncertainties deriving from pion contamination into the kaon sample

57

Uncertainty source	Average relative systematic uncertainty
Beam polarization	2.9%
Acceptance and bin migration	2.7%
Radiative effects	3.0%
Fiducial cuts	$\sim 0.0\%$
π^- contamination on e^-	$\sim 0.0\%$
Results extraction method	$\sim 0.0\%$
Systematic excluding RICH	5.0%
~~Average $\pi^{\pm}$ contamination on K^+~~	$2.0\%(1.0 \div 2.6\%)$
Global systematic	5.4%

Table 3.1: Recap of the contribution to the systematic uncertainty.

3.4 Results

The analysis is still partially incomplete because the Pass2 data became available only after summer 2023[2]. However, the aim of this study was to show that the BSA exists for kaons and it is detectable at CLAS12, and that an efficient PID ~~system~~ introduces only ~~small~~ systematic uncertainty on the measurement. ~~The~~ analogous analysis was performed on data taken from CLAS12 RG-A, which ran the experiment in ~~similar condition rather than~~ RG-B but using a hydrogen ~~target~~ instead of deuterium. The results from RG-A data are shown in Appendix A.

3.4.1 One-dimensional results

The one-dimensional results are shown as a function ~~of one~~ of the electron and kaon variables in Figures 3.11, 3.12, 3.13, and 3.14. They show that the asymmetry is detectable using the CLAS12 spectrometer for kaons identified by the RICH. The red area ~~describes the effect of~~ the total systematic uncertainty, which is a second-order effect with respect to the statistical uncertainty. Despite the limited statistical precision, the plots show the asymmetry tends to ~~be~~ zero for ~~small~~ z and p_T, as expected from theory.

3.4.2 Four-dimensional results

A four-dimensional binning was applied to the kaon sample because multidimensional analysis can provide useful information to constrain the theoretical models. The binning procedure was made ~~of~~ two steps: the sample is divided into three bins ~~in~~ the electrons variables, which are represented in Figure 3.15a, and ~~then~~ each of them is divided into four or six bins in the hadron

---

[2]The work will not remain unfinished. It was not possible to complete it before the end of the Ph.D., but the author will continue to work with the CLAS12 data and conclude the analysis, aiming to achieve a publication.
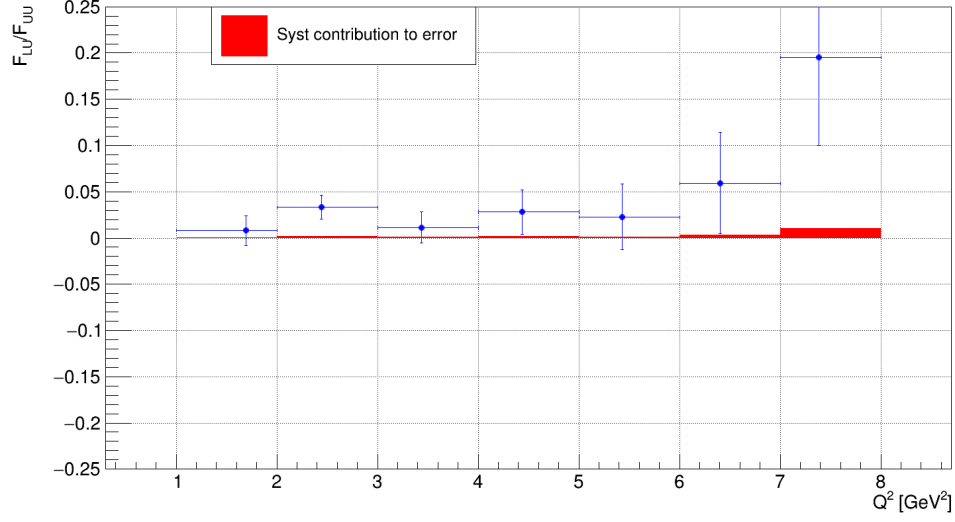
Figure 3.11: $F_{LU}^{\sin\phi}/F_{UU}$ as a function of Q^2. The red area shows the contribution of the total systematic uncertainty to the measurement error.
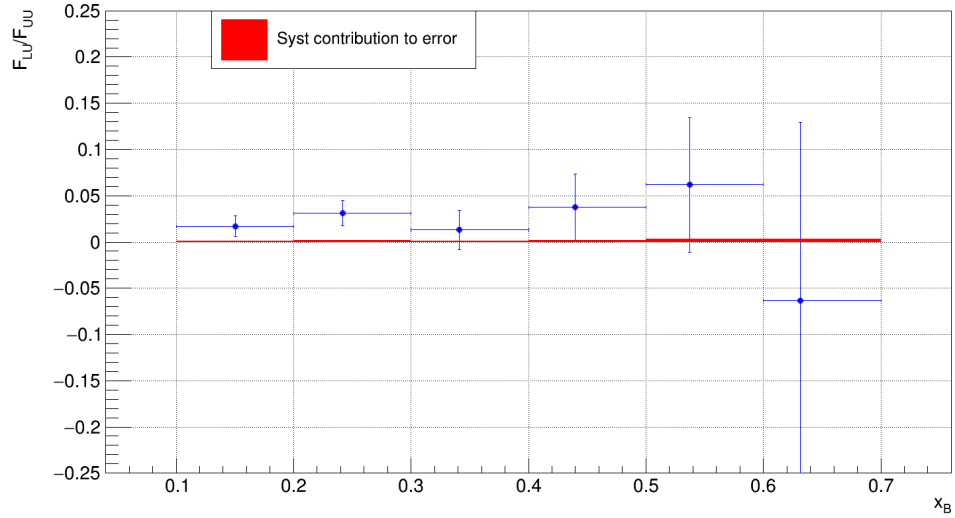

Figure 3.12: $F_{LU}^{\sin\phi}/F_{UU}$ as a function of x_B. The red area shows the contribution of the total systematic uncertainty to the measurement error.
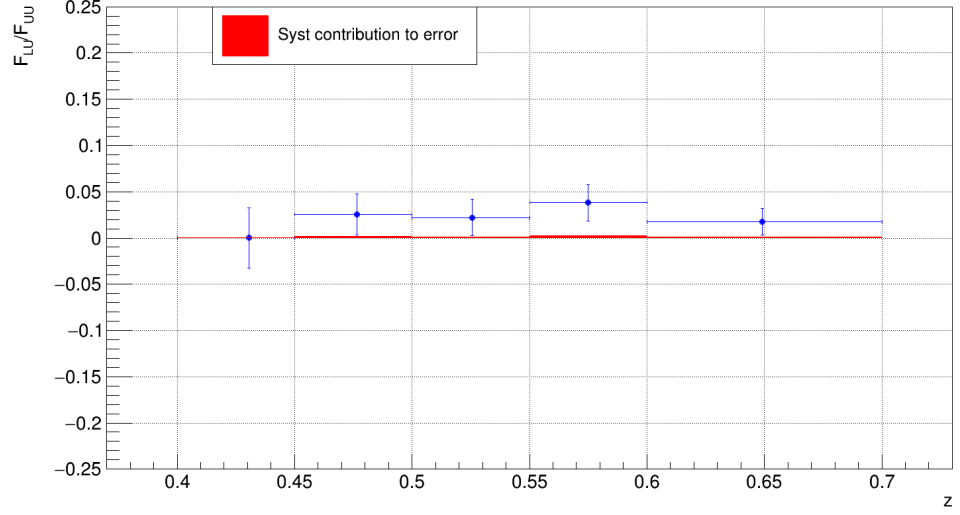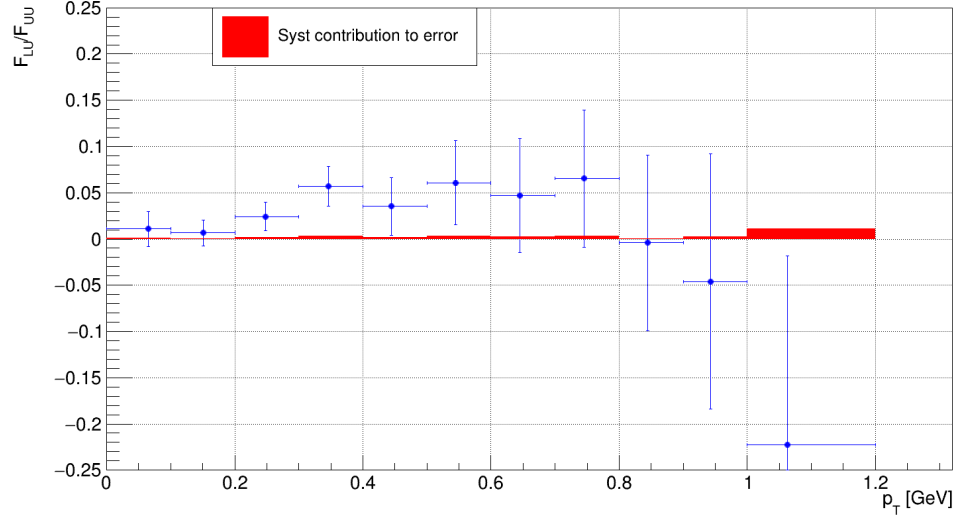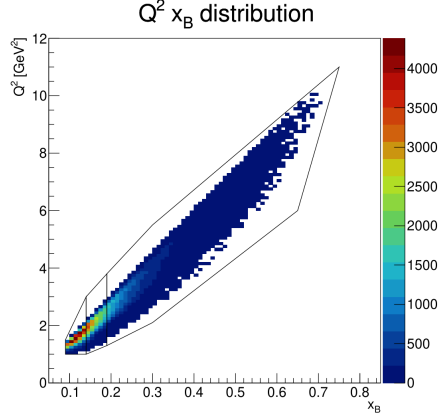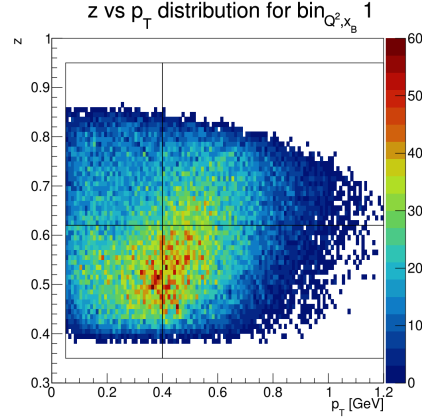
Figure 3.13: $F_{LU}^{\sin\phi}/F_{UU}$ as a function of z. The red area shows the contribution of the total systematic uncertainty to the measurement error.

Figure 3.14: $F_{LU}^{\sin\phi}/F_{UU}$ as a function of p_T. The red area shows the contribution of the total systematic uncertainty to the measurement error.

(a) Binning applied to the Q^2, x_B variables for kaons.

(b) Binning applied to the z, p_T variables for the first bin of Q^2, x_B.
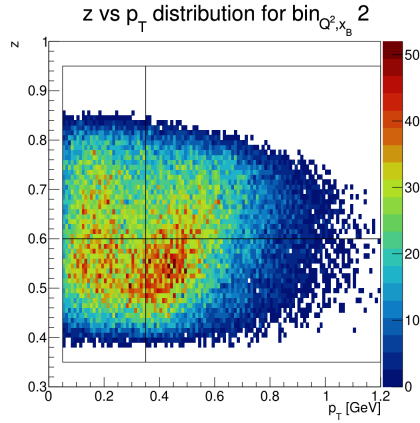
(c) Binning applied to the z, p_T variables for the second bin of Q^2, x_B.
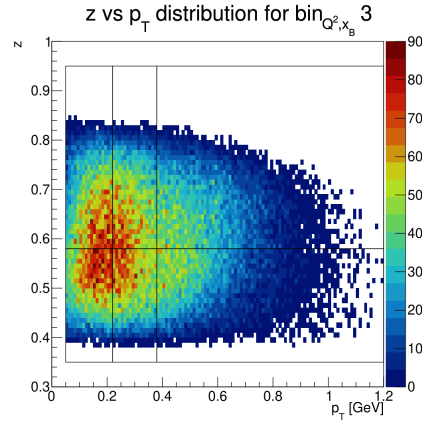
(d) Binning applied to the z, p_T variables for the third bin of Q^2, x_B.

Figure 3.15: Distribution of events in the four-dimension of interest.

variables, as shown in Figures 3.15b, 3.15c, and 3.15d. The main criteria ~~to define the binning~~ were to maximize the number of bins ~~and~~ maintain sufficient statistics in the order of $\sim 10^4$ events/bin.

The results ~~for~~ ~~the bins~~ in the electron variables and ~~the correspondent bins in~~ z are ~~expressed as a function of~~ p_T ~~and~~ shown in Figures 3.16, 3.17, and 3.18. The plots show a behavior more consistent with theory for higher Q^2 bins, ~~on which~~ the asymmetry tends to zero for small p_T and z, but the statistical error remains large. Increasing the statistics and the phase space in the future will provide possibilities to make more definitive conclusions.
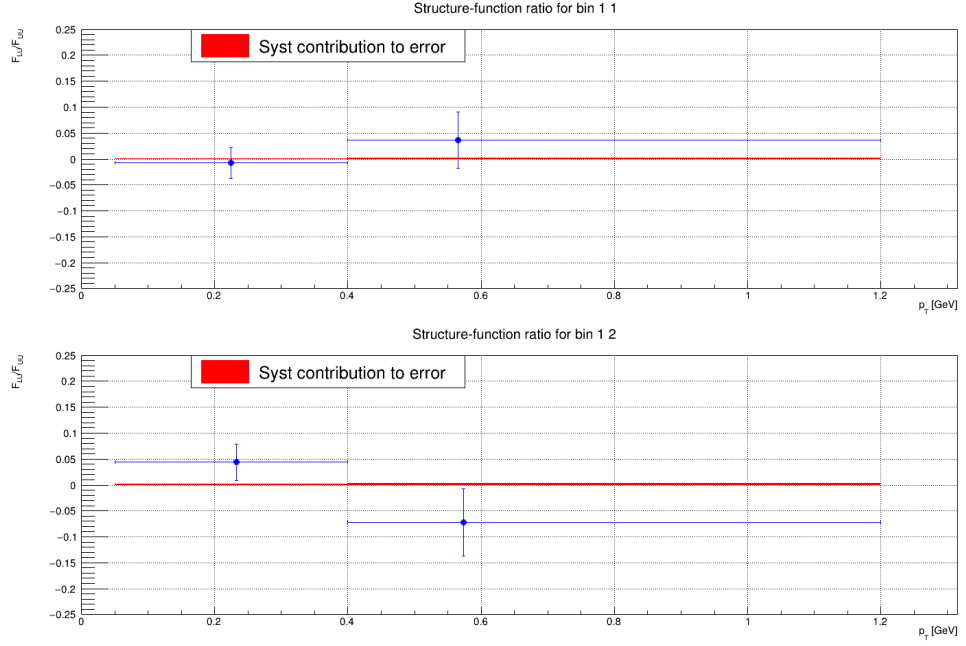
61

Figure 3.16: $F_{LU}^{\sin\phi}$ as a function of p_T, for the first bin on the electron variables and the two bins in z.
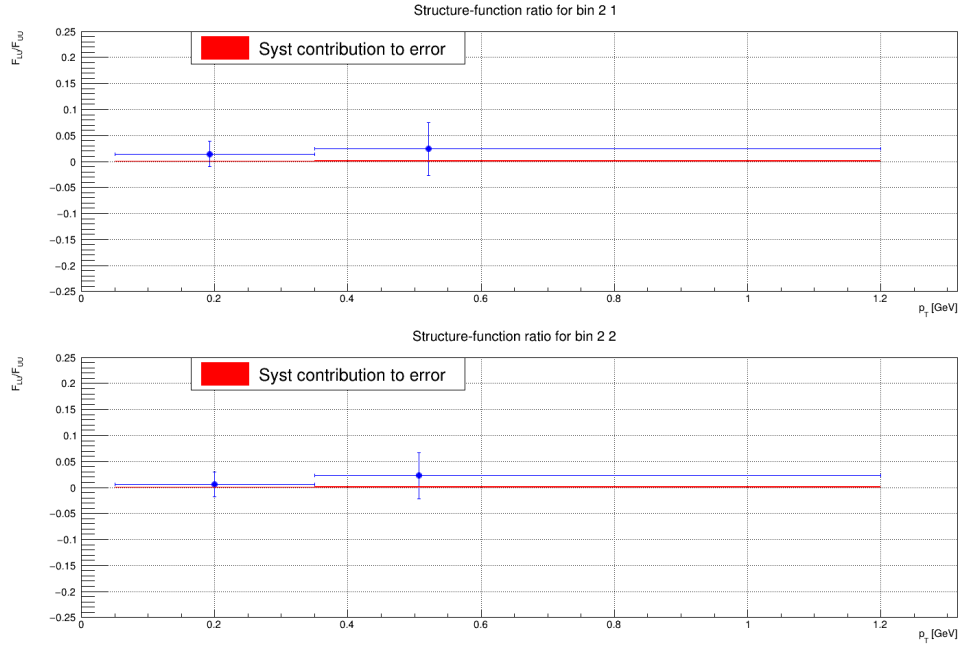

Figure 3.17: $F_{LU}^{\sin\phi}$ as a function of p_T, for the second bin on the electron variables and the two bins in z.
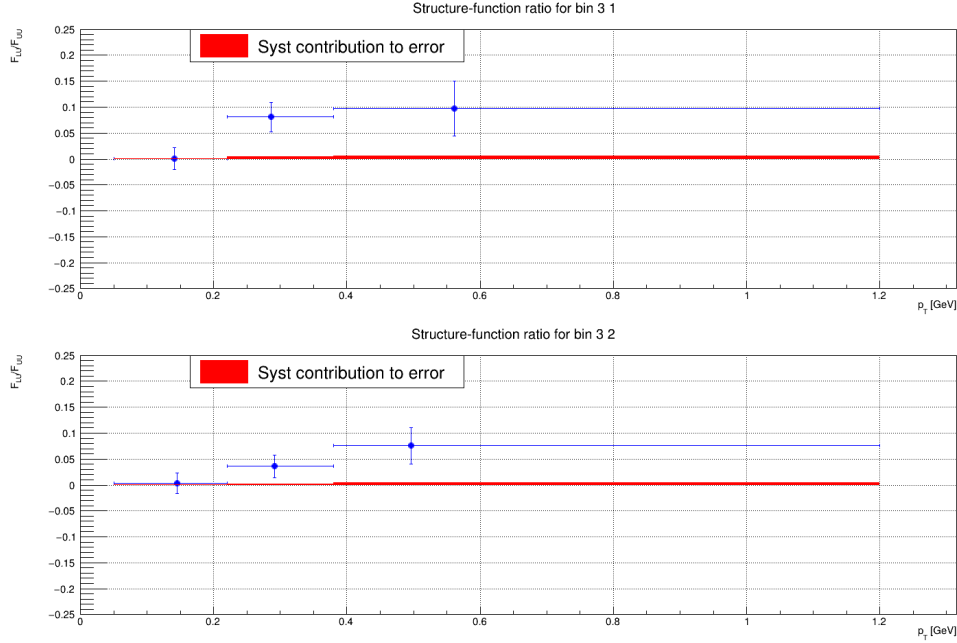
Figure 3.18: $F_{LU}^{\sin\phi}$ as a function of p_T, for the third bin on the electron variables and the two bins in z.

3.4.3 Comparison between pion and kaon

It is possible to ~~measure~~ the $F_{LU}^{\sin\phi}$ structure-function ~~both analyzing~~ pion and kaon ~~SIDIS.~~ The pion sample was selected ~~so that~~ the hadron ~~was~~ identified by the RICH, to obtain a phase space comparable with the kaon sample. All the selection criteria previously described for the ~~pion~~ sample were ~~used~~. The two samples had different statistics, as shown in Figure 3.19, showing the distributions of pions and kaons and their ratio with respect to the total. The error bars were obtained by adding in quadrature of the statistical error and the systematic error introduced by the RICH derived from the efficiency measurement in Section 2.4. The plots show that the composition of the hadron samples passing the SIDIS cuts is quite stable, except for the low-statistic region of polar angle larger than 13°, with pions that are approximately four times the number of kaons.

The one-dimensional comparison of the structure-function obtained from pion and kaon is shown in Figure 3.20. Generally, the results obtained ~~from~~ analyzing the two samples are close, but especially the kaon~~s~~ are dominated by the statistical uncertainty. More reliable results could be obtained in future studies with the completion of the RICH alignment extending the ~~polar~~ angle range up to the design~~-~~26° and analyzing the full statistics.
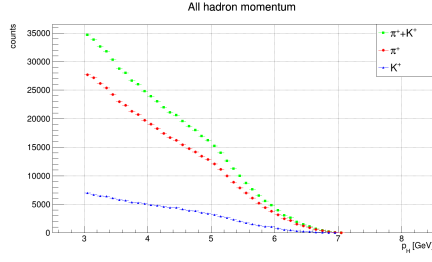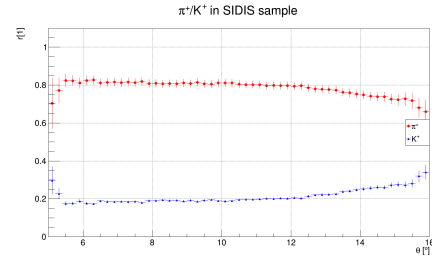
(a) Distribution of pions and kaons as a function of momentum.
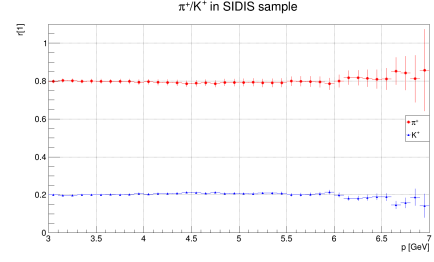
(b) Ratio of pions and kaons over the full sample as a function of momentum. The small statistics bins were excluded.
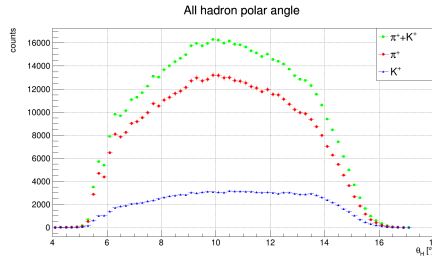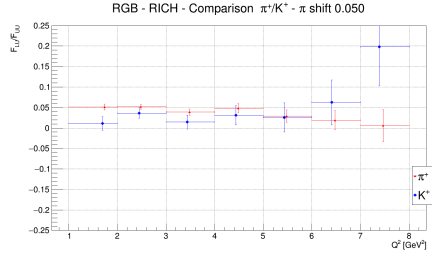

(c) Distribution of pions and kaons as a function of polar angle.
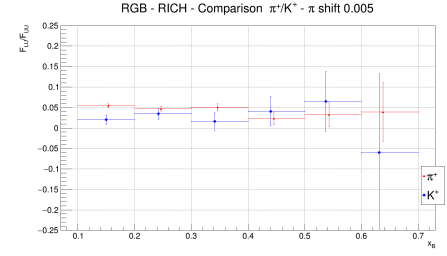

(d) Ratio of pions and kaons over the full sample as a function of polar angle. The small statistics bins were excluded.
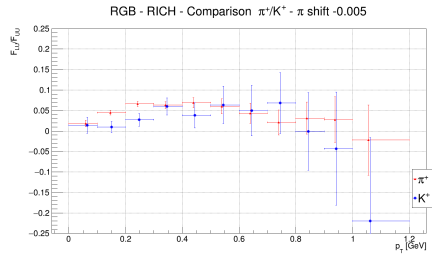
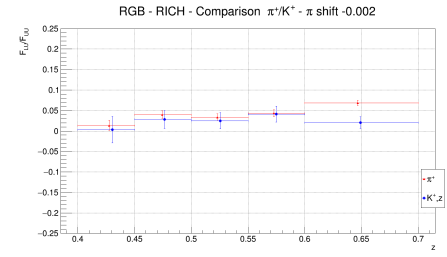**Figure 3.19:** Study of pions and kaons SIDIS sample.

(a) Comparison as a function of Q^2.

(b) Comparison as a function of x_B.

(c) Comparison as a function of p_T.

(d) Comparison as a function of z.

Figure 3.20: $F_{LU}^{\sin\phi}/F_{UU}$ obtained from pion and kaon samples identified by the RICH. The points for pion are slightly shifted along the x-axis to not overlap the error bars
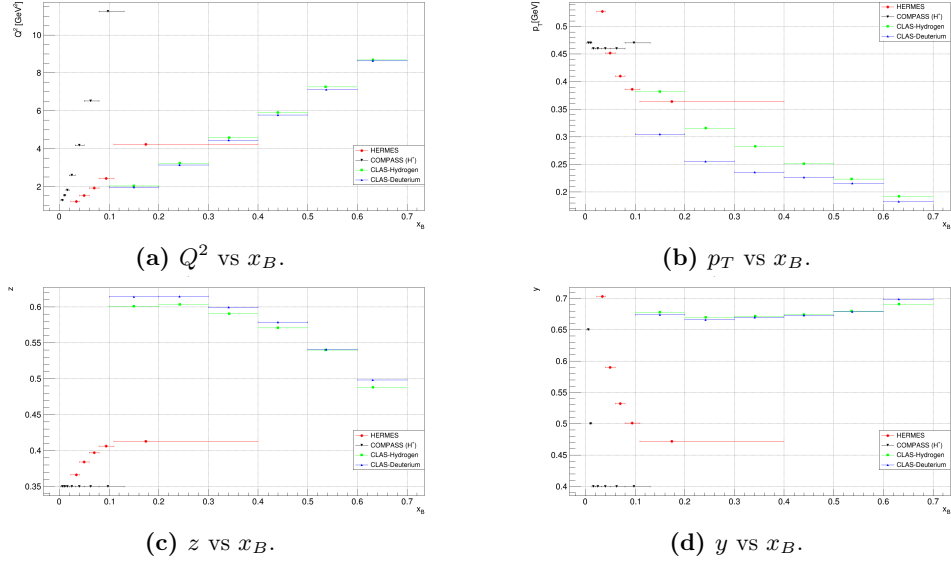
(a) Q^2 vs x_B.

(b) p_T vs x_B.

(c) z vs x_B.

(d) y vs x_B.

Figure 3.21: Trends of the kinematic variables Q^2, p_T, z, and y as a function of x_B for the results of experiments COMPASS, HERMES, and CLAS12.

3.4.4   Comparison with literature results

A preliminary comparison with ~~literature results~~ was done with HERMES measurement from Reference [27] and COMPASS measurement from Reference [22]. The results from HERMES are specifically obtained from kaon SIDIS, while COMPASS ~~mixed the positive~~ hadrons.

The mean values of kinematic variables are reported in Figures 3.21, 3.23, and 3.25. They show the capability of CLAS12 to extend the phase space to a higher x_B region. The kinematic regions are not ~~totally~~ comparable, ~~then~~ more interesting information ~~could be obtained by completing the multi-dimensional analysis~~ by running over all the available statistics and extending the kinematic region covered by the ~~CLAS12~~ RICH when the software alignment will be completed.

The structure-function comparison are shown in Figure 3.22, 3.24, and 3.26. ~~The~~ results ~~shown do not contradict~~ the measurement of HERMES and COMPASS, and for several bins, show that the high-luminosity of CLAS12 ~~allowed for a small~~ reduction of the statistical error. The addition of the second RICH module ~~will allow in the future~~ to further reduce the impact of statistical error on kaon SIDIS measurement, allowing to obtain high-precision information to constraint theoretical models.
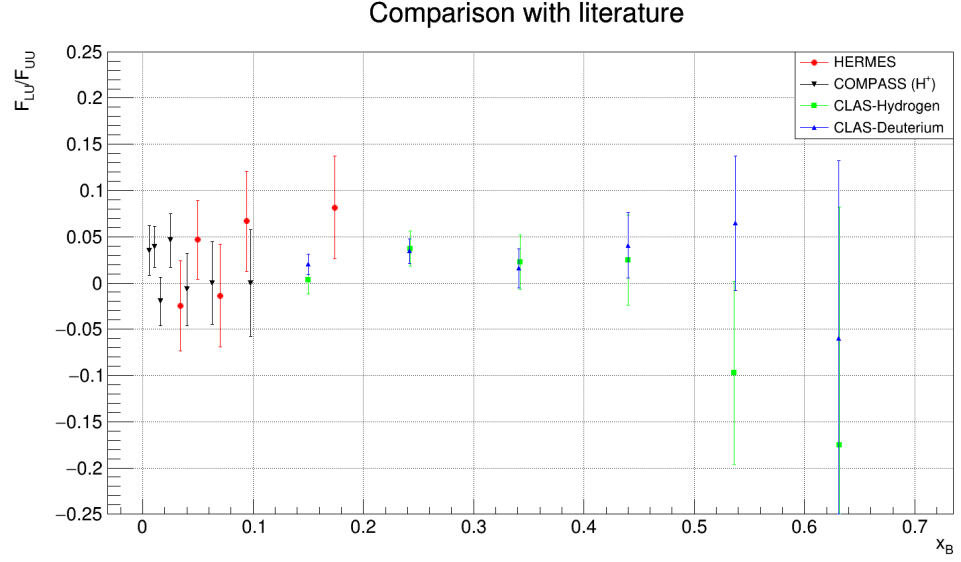
65

Figure 3.22: Structure-function measured from COMPASS, HERMES, and CLAS12 RG-A and RG-B, expressed as a function of x_B. The bin width bars were removed to make the plot more readable; they are the same as shown in Figure 3.21.
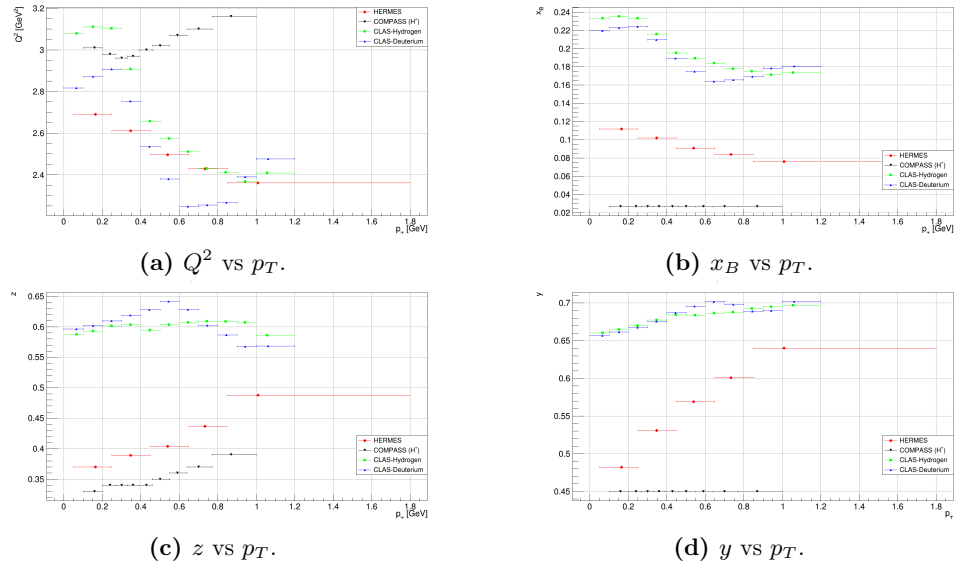

(a) Q^2 vs p_T.

(b) x_B vs p_T.

(c) z vs p_T.

(d) y vs p_T.

Figure 3.23: Trends of the kinematic variables Q^2, x_B, z, and y as a function of p_T for the results of experiments COMPASS, HERMES, and CLAS12.
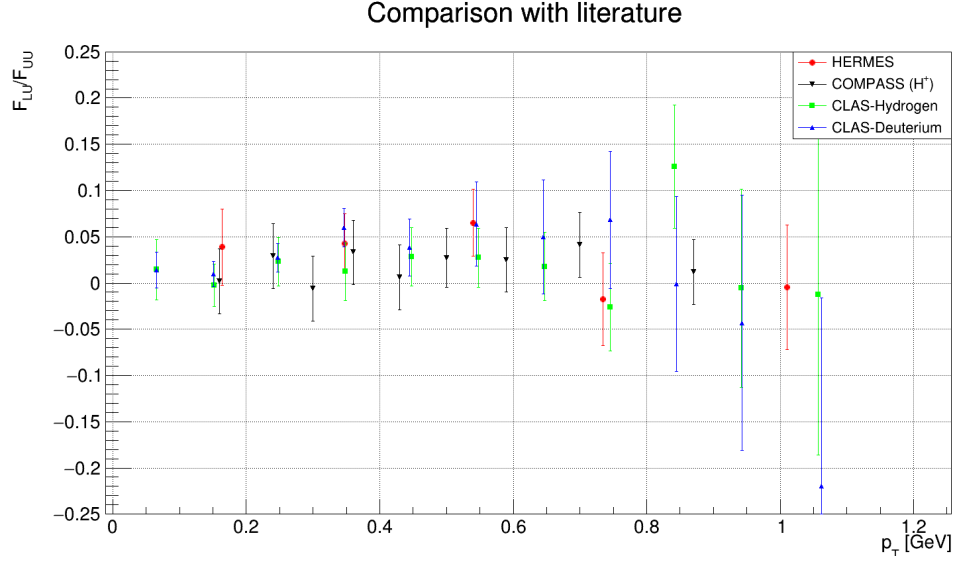
Figure 3.24: Structure-function measured from COMPASS, HERMES, and CLAS12 RG-A and RG-B, expressed as a function of p_T. The bin width bars were removed to make the plot more readable; they are the same as shown in Figure 3.23.

(a) Q^2 vs z.

(b) x_B vs z.

(c) p_T vs z.

(d) y vs z.

Figure 3.25: Trends of the kinematic variables Q^2, x_B, p_T, and y as a function of z for the results of experiments COMPASS, HERMES, and CLAS12.

67

Figure 3.26: Structure-function measured from COMPASS, HERMES, and CLAS12 RG-A and RG-B, expressed as a function of z. The bin width bars were removed to make the plot more readable; they are the same as shown in Figure 3.25.
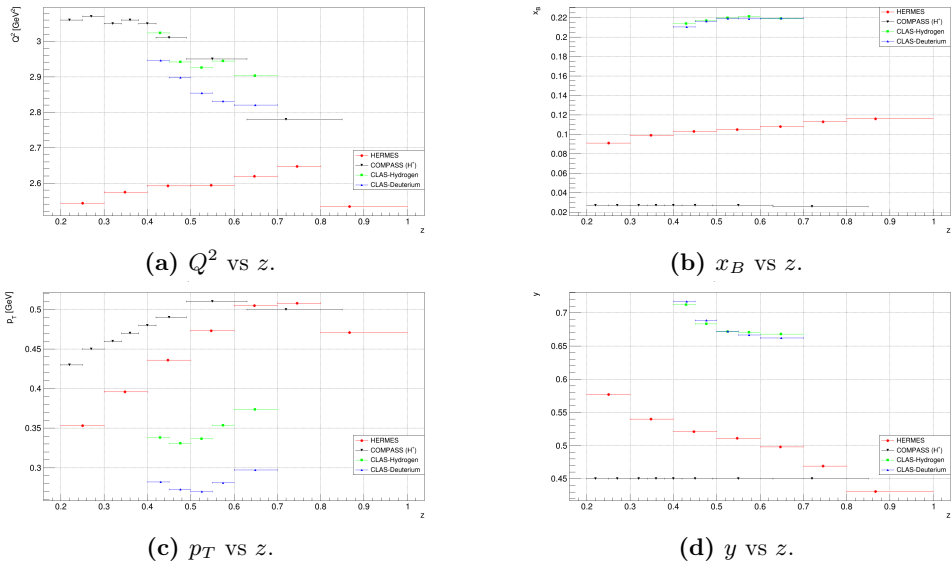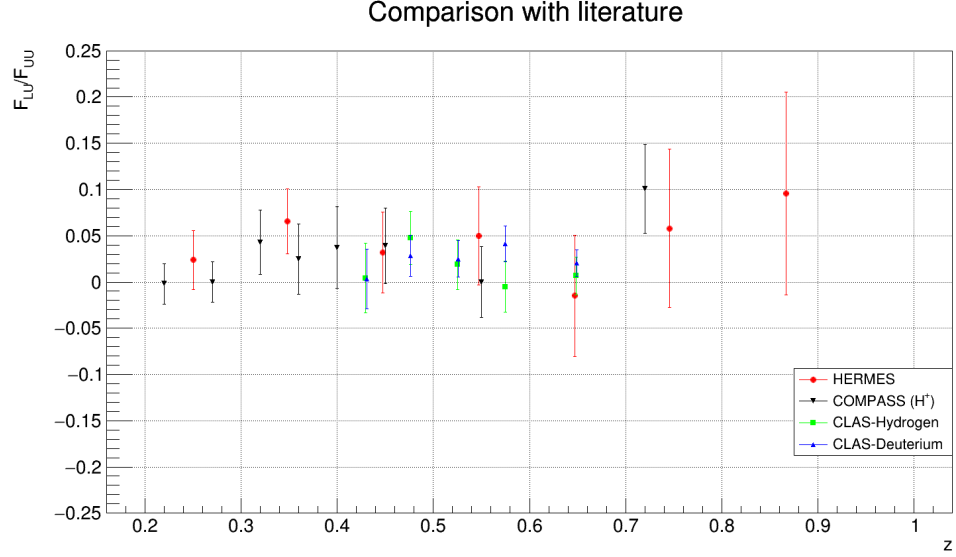
3.4.5 Future SIDIS studies using the CLAS12 RICH

This Chapter showed ~~it~~ is possible to extract ~~an asymmetry for kaon~~ despite the limited statistics analyzed. In the immediate future, the analysis will be extended to the full sample of recorded data on deuterium, including several runs acquired with the torus in opposite polarization. Moreover, the completion of the RICH alignment-possible with the Pass2 reconstruction software-will permit-almost double the phase space covered up to the ~~expected~~ value of 26° in polar angle. To ultimate the measurement, the data for kaons with momentum lower than 3 GeV, identified by the standard CLAS12 PID, can be ~~added~~ to further extend the phase space. The addition of the second module of the detector, which occurred in 2022, will increase the available statistics, allowing us to divide the data in more dense bins, providing more information to constrain the TMDs.

This study demonstrates the capability of the RICH ~~in~~ efficiently identify ~~the~~ hadrons in the high-momentum range of CLAS12, between 3 GeV/c and 8 GeV/c. RICH information will help several studies that are ongoing on kaons, like the measurement of other terms of the SIDIS cross-section or the dihadron spin-asymmetries including at least one kaon. Moreover, the study of the high-momentum SIDIS kaons provides access to the high z region, and to the possibility of ancillary investigations, for example, about the role of vector mesons.